Mechanistic Insight into the Catalytic Promiscuity of Amine Dehydrogenases: Asymmetric Synthesis of Secondary and Primary Amines

Vasilis Tseliou, Marcelo F. Masman, Wesley Böhmer, Tanja Knaus, and Francesco G. Mutti*[a]

Biocatalytic asymmetric amination of ketones, by using amine dehydrogenases (AmDHs) or transaminases, is an efficient method for the synthesis of α-chiral primary amines. A major challenge is to extend amination to the synthesis of secondary and tertiary amines. Herein, for the first time, it is shown that AmDHs are capable of accepting other amine donors, thus giving access to enantioenriched secondary amines with conversions up to 43%. Surprisingly, in several cases, the promiscuous formation of enantiopure primary amines, along with the expected secondary amines, was observed. By conducting practical laboratory experiments and computational experiments, it is proposed that the promiscuous formation of primary amines along with secondary amines is due to an unprecedented nicotinamide (NAD)-dependent formal transamination catalysed by AmDHs. In nature, this type of mechanism is commonly performed by pyridoxal 5′-phosphate aminotransferase and not by dehydrogenases. Finally, a catalytic pathway that rationalises the promiscuous NAD-dependent formal transamination activity and explains the formation of the observed mixture of products is proposed. This work increases the understanding of the catalytic mechanism of NAD-dependent aminating enzymes, such as AmDHs, and will aid further research into the rational engineering of oxidoreductases for the synthesis of α-chiral secondary and tertiary amines.

Introduction

Catalytic enzyme promiscuity is the ability of an enzyme to catalyse alternative chemical reactions often by following catalytic mechanisms that are different from the natural one.[1] Although catalytic enzyme promiscuity has been the object of intensive investigation for two decades, the discovery of new promiscuous activities still proceeds at regular pace, as witnessed by recent publications.[2] Notably, these new biocatalytic activities have been frequently exploited in chemical synthesis.

Amine dehydrogenases (AmDHs) catalyse the reductive amination of carbonyl compounds at the expense of aqueous ammonium/ammonia (a) buffer. All known AmDHs, to date, were obtained mainly by protein engineering, starting from α-amino acid dehydrogenases, such as leucine dehydrogenases from *Bacillus stereothermophilus*,[3] *Exiguobacterium sibiricum*,[4] *Lysinibacillus fusiformis*[5] and *Bacillus sphaericus*,[5] as well as phenylalanine dehydrogenases from *Bacillus badius*,[6] *Rhodococcus* sp.

M4[7] and *Caldalkalibacillus thermarum*.[8] In all of these cases, mutations of the highly conserved lysine and asparagine residues in the active site, which interact with the two oxygen atoms of the carboxylic moiety of the natural substrate, were essential for switching the substrate specificity from α-keto carboxylic acids to ketones.[3,6–8] A few native AmDHs have been identified from *Petrotoga mobilis*, *Fervidobacterium nodosum*, *Clostridium sticklandii*, *Dethiosulfovibrio peptidovorans*, *Staphylothermus hellenicus* and *Thermosediminibacter oceani*.[9] Several studies on asymmetric biocatalytic reductive amination by using the above-mentioned AmDHs have been published very recently through the use of isolated enzymes, immobilised enzymes or whole-cell biocatalysts.[3–10] In particular, our group showed that AmDHs are efficient catalysts for the reductive amination of prochiral ketones (i.e., turnover numbers (TONs) $> 10^3$) and their substrate scope already covers a respectable range of structurally diverse substrates.[10d] Biocatalytic reductive amination is also possible with imine reductases (IReds), which naturally catalyse the asymmetric reduction of cyclic imines.[11] During the past few years, various groups have shown that IReds are also capable of catalysing the reductive amination of non-cyclic imines, although with modest efficiency.[12] In a recent study, the reductive amination between ketones and small aliphatic and benzylic amines was performed with a novel dehydrogenase from *Aspergillus o.* (AspRedAm).[13] The enzyme was classified as a "reductive aminase" (RedAm). In a follow-up study, two additional RedAms were characterised.[14] Finally, a previous patent from Codexis reported a RedAm activity from a library of variants originating from an opine dehydrogenase (ODH).[15]

[a] V. Tseliou, Dr. M. F. Masman, W. Böhmer, Dr. T. Knaus, Prof. Dr. F. G. Mutti
van 't Hoff Institute for Molecular Sciences
HIMS-Biocat, University of Amsterdam
Science Park 904, 1098 XH Amsterdam (The Netherlands)
E-mail: f.mutti@uva.nl

This article is part of the young researchers' issue ChemBioTalents. To view the complete issue, visit: http://chembiochem.org/chembiotalents

Despite differences in names and apparent reactivity, the catalytic mechanisms of IReds, AmDHs and RedAm are closely related because the actual mechanism is essentially based on hydride transfer from the nicotinamide adenine dinucleotide (NADH) or nicotinamide adenine dinucleotide phosphate (NADPH) coenzyme to the in situ formed imine intermediate or already existing cyclic imine in solution. Thus, we hypothesised that the reactivity of AmDHs may not be restricted only to **a** as an amine donor, as previously believed and reviewed elsewhere.[11b] This was also suggested by a number of oxidoreductases present in nature, such as ODHs, which are capable of generating secondary amines through the coupling of an α-amino acid with an α-keto acid.[16]

Herein, we show, for the first time, that the reactivity of AmDHs is indeed not limited to **a** as the amine donor. The two AmDHs considered herein can accept other amine donors to enable the formation of secondary and tertiary amines. Surprisingly, in some cases, the reaction was accompanied by the promiscuous formation of primary amines, along with the expected secondary and tertiary amines. With the aim of explaining such unprecedented promiscuous activity, as well as the stereoselective outcome of the reaction, we performed a study based on an accurate combination of practical laboratory experiments and computational studies. Consequently, herein we also propose a catalytic cycle for AmDHs, which explains the promiscuous formation of all products (that is, secondary and primary amines) and the enantiomeric composition of the reaction mixture.

Results and Discussion

Screening of carbonyl compounds and amine donors

The reactivities of Rs-AmDH (originating from the enzyme engineering of phenylalanine dehydrogenases from *Rhodococcus* sp. M4)[7,10d] and Ch1-AmDH[10b,d] (a chimeric enzyme obtained through domain shuffling of first-generation variants) were assayed with 11 different amine donors, which also constituted the buffer system. Four different types of carbonyl compounds were selected: aliphatic ketones, aromatic ketones, aliphatic al-

Francesco Mutti obtained his Master's degree in industrial chemistry *summa cum laude* (2004) and his Ph.D. in chemistry (2008) from the University of Milan. After post-doctoral work in the groups of Prof. Wolfgang Kroutil at the University of Graz (2009–2012) and Prof. Nicholas Turner at The University of Manchester (2013–2014), he moved to the University of Amsterdam (2015). He has published 40 research papers, several book chapters and 4 patents. His research interests are in the area of biocatalysis—developing biocatalytic cascades for the sustainable manufacture of chemical products—enzyme discovery, and enzyme engineering.
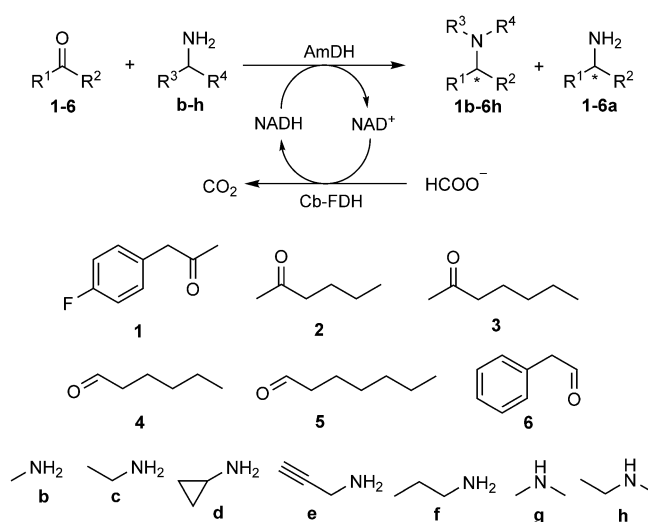
Scheme 1. Biocatalytic reductive amination of carbonyl compounds (**1–6**, 10 mM) with different amine donors (**b–h**) catalysed by N-terminal His$_6$-tagged AmDHs. The amine donor was also used as a buffer species in water for the reaction (1 M, pH 8.5, formate as counter-anion). The NAD$^+$ coenzyme (1 mM) was recycled by reduction with formate; this was catalysed by N-terminal His$_6$-tagged formate dehydrogenase from *Candida boidinii* (Cb-FDH). The amination reaction generated the following secondary or tertiary amines (**1 b–d**, **2 b**, **3 b**, **4 b**, **5 e**, **6 b,c**, **6 f–h**), along with the unexpected formation of the following structurally related primary amines (**1–3 a**). For full experimental screening, see Table S1.

dehydes and aromatic aldehydes (Scheme 1; for a complete list of carbonyl compounds and amine donors, see Figures S1 and S2 in the Supporting Information). We conducted the initial biocatalytic reactions as follows: carbonyl compound (10 mM), amine/aminium formate buffer (1 M, pH 8.5), N-terminal His$_6$-tagged Rs-AmDH (>99% purity, 103 μM, 1 mol%) or N-terminal His$_6$-tagged Ch1-AmDH (>99% purity, 92 μM, 0.9 mol%), NAD$^+$ (1 mM) and N-terminal His$_6$-tagged Cb-FDH (>99% purity, 24 μM, 0.2 mol%; for recycling of NADH), at ambient temperature, for 48 h.

Under the above-mentioned reactions conditions, both tested AmDHs produced secondary or tertiary amines from ketones and aldehydes (for a complete list of products, see Figure S3). Selected results are reported in Table 1; all screening results are reported in Table S1. Ch1-AmDH catalysed the reductive amination between 4′-fluorophenylacetone (**1**) and methylamine (**b**), whereas Rs-PhAmDH accepted ketone **1** in combination with ethylamine (**c**) and cyclopropylamine (**d**; Table 1, entries 1, 3 and 4). For these reactions, we were surprised to identify the formation of the structurally related primary amine, 4′-fluoroamphetamine (**1 a**), as a second product. Notably, product **1 a** was obtained in enantiopure form in all cases (>99% *R*). A commercial reagent grade solution of **b** contains only negligible traces of **a**, whereas **c** and **d** do not contain **a** at all. In addition, the amination of **1** at 4–6 M concentration of **b** as a buffer resulted in lower conversion into **1 a**, compared with the same reaction performed at 3 M **b** (Figure 1B). Hence, we ruled out the possibility that the primary amine could have been formed through the enzymatic reaction between the ketone and **a** present as an impurity. Due to

Table 1. Reductive amination reactions performed by AmDHs for the synthesis of secondary and tertiary amines. Standard reaction conditions: substrate (10 mM), N-terminal His$_6$-tagged Ch1-AmDH (>99% purity, 92 μM, 0.9 mol%) or N-terminal His$_6$-tagged Rs-AmDH (>99% purity, 103 μM, 1 mol%), N-terminal His$_6$-tagged Cb-FDH (>99% purity, 24 μM, 0.2 mol%) and buffer constituted by amine donor with formate as counter-anion (1 M, pH 8.5). The reactions were performed at 30°C, for 48 h using an orbital shaker at 170 rpm.

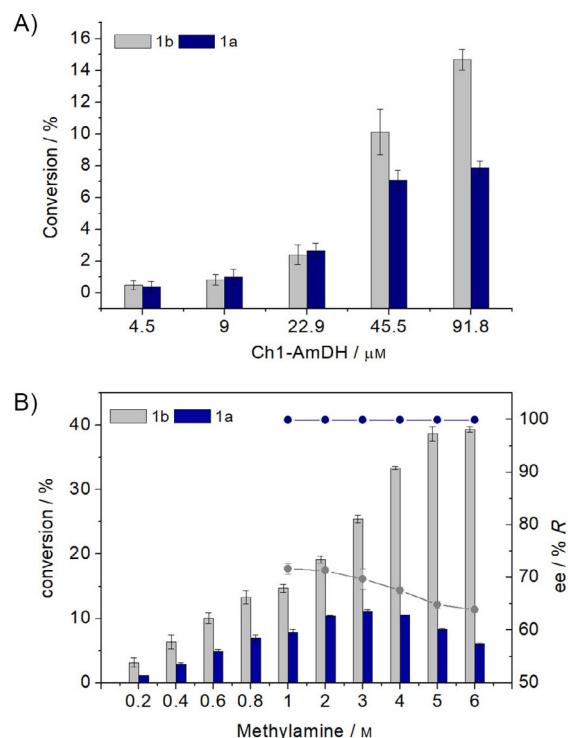|	Substrate	Amine donor	AmDH	Secondary amine Conv. [%][b]	Secondary amine ee [%][c]	Primary amine (1–11 a) Conv. [%][b]	Primary amine (1–11 a) ee [%][c]
1	1	b	Ch1	15	72 (R)	8.	>99 (R)
2	1	b	Ch1	40[a]	64 (R)	6	>99 (R)
3	1	c	Rs	4	n.m.	26	>99 (R)
4	1	d	Rs	11	1 (R)	26	>99 (R)
5	2	b	Ch1	5	n.m.	4	>92 (R)[d]
6	3	b	Ch1	32	n.m.	26	>99 (R)
7	4	b	Rs	24	n.a.	n.d.	n.a.
8	5	e	Ch1	41	n.a.	n.d	n.a.
9	6	b	Rs	29	n.a.	n.d	n.a.
10	6	c	Rs	40	n.a.	n.d	n.a.
11	6	f	Rs	43	n.a.	n.d	n.a.
12	6	g	Rs	3[e]	n.a.	n.d	n.a.
13	6	h	Rs	8[e]	n.a.	n.d	n.a.

[a] Concentration of MeNH$_2$/MeNH$_3^+$ buffer was increased to 6 M. [b], [c] For analytical determination of conversions and enantiomeric excess (ee) values, see the Supporting Information, paragraphs 8–10. [d] Unable to be determined with precision, due to experimental noise of the GC traces. [e] Measured by means of GC-MS.

Figure 1. A) Dependence of enzyme concentration (>99% purity, 4.5–91 μM, equal to 0.045–0.9 mol%) at fixed concentrations of **b** as a buffer (1 M) for the conversion of **1** into primary (**1 a**, blue columns) and secondary (**1 b**, grey columns) amines catalysed by N-terminal His$_6$-tagged Ch1-AmDH. A catalytic amount of NAD$^+$ (1 mM) was applied and recycled by using N-terminal His$_6$-tagged Cb-FDH (>99% purity, 24 μM, 0.2 mol%). Error bars represent the standard deviation calculated from three independent experiments. B) Dependence of CH$_3$NH$_2$ concentration (200 mM to 6 M) at a fixed concentration of N-terminal His$_6$-tagged Ch1-AmDH (>99% purity, 91 μM, 0.9 mol%) for the conversion of **1** into primary (**1 a**, purple columns) and secondary (**1 b**, grey columns) amines catalysed by Ch1-AmDH. A catalytic amount of NAD$^+$ (1 mM) was applied and recycled by using N-terminal His$_6$-tagged Cb-FDH (>99% purity, 24 μM, 0.2 mol%). Error bars represent the standard deviation from three independent experiments. The ee values for **1 a** (blue) and **1 b** (grey) are depicted as circles connected by a solid line.

the complexity and elevated polarity of the components in the reaction mixtures, we succeeded in measuring the ee of the secondary amine products by chromatography in the case of compounds **1 b** and **1 d**. Compound **1 b** was obtained in enantioenriched form (72% R; Table 1, entry 1), whereas **1 d** was in nearly racemic form (Table 1, entry 4). In contrast, the other product—primary amine **1 a**—was obtained in enantiopure form, as previously observed (for comparison, Table 1, entries 1 and 4).

Ch1-AmDH was the most active enzyme for the amination of hexan-2-one (**2**) and heptan-2-one (**3**) with **b** (Table 1, entries 5 and 6). Even in this case, the structurally related primary amines 2-aminohexane (**2 a**) and 2-aminoheptane (**3 a**) were obtained with perfect ee. These results confirm that the formation of primary amines occurs during the catalytic cycle of the AmDHs. Conversely, the amination of aldehydes with the AmDHs and different amine donors under our initial reaction conditions (1 M amine/aminium buffer, pH 8.5), proceeded with perfect chemoselectivity to afford the expected secondary amines as the sole product in up to 43% conversion (Table 1, entry 7–11). As a proof of principle, the amination was run also with secondary amines as amine donor (for example, dimethylamine, ethylmethylamine), leading to tertiary amines, albeit with poor conversions (Table 1, entry 12 and 13).

Influence of the enzyme and amine donor concentration

For further studies, we selected the amination of **1** with **b** as a test reaction. In the first set of experiments, we kept the buffer concentration constant (1 M, pH 8.5) and we varied the concen-

tration of N-terminal His$_6$-tagged Ch1-AmDH (>99% purity, 4.5–91 μM, equal to 0.045–0.9 mol%). As expected, increasing the enzyme concentration affected the overall conversion positively (Figure 1 A and Table S2). Interestingly, the ratio between the formation of secondary (**1 b**) and primary (**1 a**) amines also varied, depending on the enzyme concentration from 1:1.2 (at AmDH 4.5 μM) to 1:1.9 (at AmDH 91 μM).

In a follow-up experiment (Figure 1 B), we fixed the concentration of N-terminal His$_6$-tagged Ch1-AmDH (>99% purity, 91 μM, 0.9 mol%) and increased the concentration of the CH$_3$NH$_2$/CH$_3$NH$_3^+$ buffer (200 mM–6 M). Increasing the buffer concentration correlated with a consistent increase in the formation of **1 b**. At 6 M buffer concentration, compound **1 b** was finally obtained in 40% conversion (Figure 1 B and Table 1 entry 2; for details see the Supporting Information, Table S3). The side reaction that led to the primary amine product showed a continuous increment of conversion of **1 a** (11% conversion) up to a buffer concentration of 3 M. Surprisingly, a more elevated concentration of buffer (4, 5, 6 M) reduced the

formation of **1a** (6% at 6 M buffer concentration). Hence, the ratio between **1a** and **1b** further increased to 1:6.6. We also monitored a possible variation in the stereoselective outcome of the reaction. The *ee* of the secondary amine product **1b** was partially affected, with a reduction from 72 (1 M buffer) to 64% *ee* (6 M buffer). In contrast, the optical purity of the primary amine remained perfect (>99%; Table 1, entries 1 and 2). In all cases, the *R*-configured amine (secondary or primary) was the favoured enantiomer.

Initial biochemical and computational studies towards an understanding of the reaction mechanism

Both Ch1-AmDH and Rs-AmDH possessed a generally perfect stereoselectivity (i.e., *R* selectivity) for the reductive amination of prochiral ketones with **a**.[10d] However, different points remained unclear at this stage: 1) the molecular discriminants that determined a productive combination between the ketone/aldehyde and the amine donor; 2) the formation of secondary amines with moderate stereoselectivity; and 3) the unexpected formation of a primary amine in enantiopure form.

Therefore, we performed several computational analyses in an attempt to elucidate these points. Firstly, we generated several models of Rs-AmDH in complex with NADH and different protonated imine intermediates (that is, carbonyl compounds: **1**, hexanal (**4**), heptanal (**5**), phenylacetaldehyde (**6**), 4-phenyl-butan-2-one (**9**), acetophenone (**10**); amine donors: **a**, **b**, **c** and *n*-propylamine (**f**)). Details on the creation of these models are reported in the Experimental Section. Based on the reported catalytic mechanism of the parent wild-type phenylalanine dehydrogenase from *Rhodococcus* sp. M4,[17] we analysed the models by considering two crucial parameters (Figure 2): 1) the distance between the departing hydride of NADH and the prochiral carbon of the imine intermediate (herein referred to as "distance 1"); and 2) the distance between the negatively charged oxygen atom of the terminal carboxylic group of Asp118 of Rs-AmDH and the hydrogen of the positively
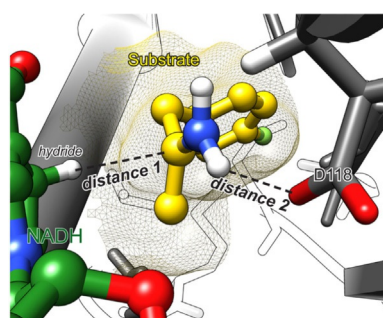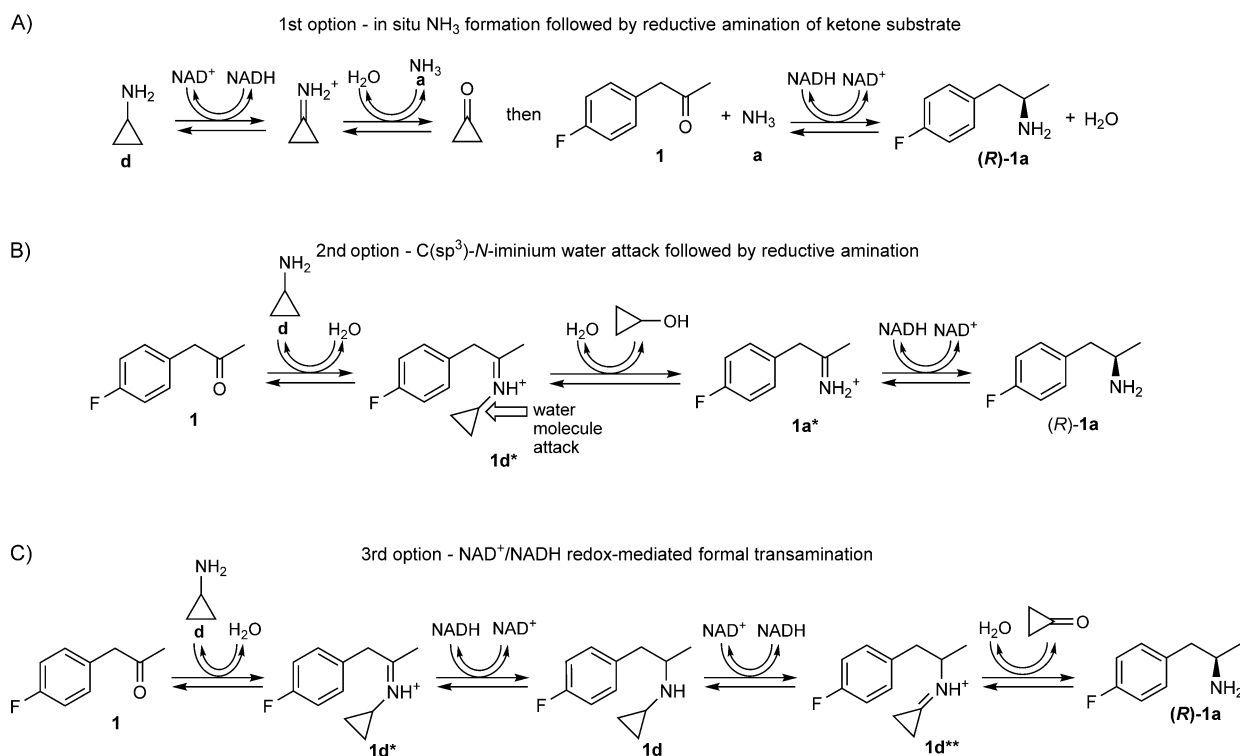

Figure 2. Simplified schematic view of the productive binding mode for the iminium intermediate in the active site of the AmDH. For clarity, only the NAD coenzyme in its reduced form (NADH) and the highly conserved amino acid residue Asp118 (numbering of Rs-AmDH) of the enzyme are indicated. The actual spatial positions and orientations of NADH, substrate and Asp118 in the active site were retained, according to our calculated model. The iminium intermediate (**1a***), which is generated by the interaction between **1** and **a**, is depicted. Critical distances 1 and 2 are depicted with a dashed black line.

charged iminium group of the intermediate (herein referred to as "distance 2").

Our analysis revealed that the highest reactivity (that is, conversion) for the reductive amination was achieved if both above-mentioned distances had an optimal value. The sum of the van der Waals (vdW) radii[18] of carbon and hydrogen can be considered as the threshold distance, which is about 2.9 Å (r_H^{vdW} = 1.2 Å, r_C^{vdW} = 1.7 Å; for details, see the Experimental Section). Thus, an optimal distance must be around or moderately below 2.9 Å. For instance, the reductive amination of **1** with **a** catalysed by Rs-AmDH was reported to proceed quickly and in a quantitative manner.[10d] Our model for this reaction with Rs-AmDH and the related iminium intermediate (**1a***) indeed displays an optimal distance 1 of 2.7 Å and an optimal distance 2 of 1.9 Å (Figure S4 A). Conversely, the same reaction between **1** and **c** affords only 4% conversion (Table 1, entry 3). In our models for the latter reaction, considering the related iminium intermediate **1c***, distance 1 is still ideal (2.9–3.0 Å), whereas distance 2 is significantly larger (4.8–6.0 Å; Figure S4 B and C). Another interesting example is the reductive amination between **10** and either **a** or **c**. The reaction with **a** as an amine donor afforded only a moderate conversion of 34% after 48 h;[10d] our model for this reaction with the related iminium intermediate **10a*** (Figure S4 D) displays an optimal distance 1 of 3.0 Å, but distance 2 is slightly elongated (3.3 Å). Conversely, the reaction between **10** and **c** did not occur at all (Table S1); in fact, although one of our models for this reaction with iminium intermediate **10b*** displays an optimal distance 2 of 3.00 Å, distance 1 is much larger (4.0 Å; Figure S4 E). Finally, 4-phenylbutan-2-one (**9**) and **a** react quantitatively within a short time.[7,10d] Our model for this reaction with iminium intermediate **9a*** shows both perfect distances 1 and 2 of 2.8 and 3 Å, respectively (Figure S4 G). In contrast, the reaction between **9** and **c** did not occur. Coherently, our models for this reaction with iminium intermediate **9c*** show a longer distance 1, ranging from 3.4 and 3.5 Å (Figure S4 H and I). A similar study conducted with aldimines as intermediates provided an analogous trend (Figure S5). In conclusion, our analysis revealed that the distance between the prochiral iminium carbon of the intermediate and the hydride of NADH (Figure 2, distance 1) is the parameter of primary importance for the reaction to occur. Nevertheless, the residue Asp118 (numbering of Rs-AmDH) appears to play a role for achieving relevant turnovers (Figure 2, distance 2). However, this analysis permits us only to rationalise which are the crucial parameters that enable the reduction of the iminium intermediate bound in the active site of an AmDH. Otherwise, the reductive amination of a prochiral ketone with different amine donors (**b**–**e**) catalysed by AmDHs generates complex reaction mixtures containing secondary amines (**1b**–**d**, **2b**, **3b**, **4b**, **5e**) with moderate optical purity and the unexpected primary amines in enantiopure form (**1**–**3a**). This observation suggests the existence of, at least, two stereocomplementary productive binding configurations for the reduction of secondary iminium intermediates.

On the other hand, because the unexpected primary amines (**1**–**3a**) were always obtained in optically pure form (>99% *R*), the promiscuous formation of these products was clearly cata-

A) 1st option - in situ NH₃ formation followed by reductive amination of ketone substrate

B) 2nd option - C(sp³)-N-iminium water attack followed by reductive amination

C) 3rd option - NAD⁺/NADH redox-mediated formal transamination

Scheme 2. Possible mechanistic explanations for the promiscuous formation of enantiopure primary amine as by-product.

lysed by the AmDHs. At this stage, we envisioned three possible reaction mechanisms that could explain the formation of primary amines (Scheme 2).

The first option (Scheme 2A) predicts an oxidative deamination of the amine donor (**b**–**d**; **d** in the example), which is catalysed by the AmDH. Free **a** generated in the first step may serve as the amino donor in a subsequent reductive amination that is always catalysed by the AmDH. The second option (Scheme 2B), which explains the formation of the enantiopure primary amine as a side product, predicts an unlikely promiscuous hydrolytic activity of AmDHs. In fact, a polarised water molecule in the active site of AmDH with appropriate orientation, may attack the sp³-carbon atom in the α position to the nitrogen of the ketiminium intermediate (**1d*** in the example). Although such a hydrolytic step is chemically unlikely, it cannot be excluded beforehand because of the particular catalytic environment in the active site of the AmDH, in which a polarised water molecule is normally involved in catalysis.[17] If such a hydrolytic step occurred, subsequent hydride transfer from NADH would generate a primary amine. Furthermore, only in the case of cyclic intermediates such as **1d***, would the same nucleophilic attack of a water molecule also provoke the opening of the cyclopropyl ring to give an aminol upon reduction (not depicted in Scheme 2B). However, this route is also incompatible with the observed mixture of products. The third option (Scheme 2C) is an unprecedented formal transamination reaction. In nature, transamination reactions are catalysed by pyridoxal 5′-phosphate (PLP)-dependent aminotransferase through a ping-pong mechanism.[19] However, an alternative NAD⁺/NADH redox-mediated mechanism is conceivable. Ac-

cording to this hypothesis, the key catalytic step would be the isomerisation of the ketiminium intermediate (**1d*** in Scheme 2C) through the action of NAD⁺/NADH, to give the other ketiminium intermediate **1d****.

One could exclude the first option (Scheme 2A) by considering the analysis of the composition of the reaction mixture after the biocatalytic reductive amination. In fact, the concentration of amine donor (**b**–**d**) remained constant, at nearly 1 M, from the beginning until the end of the reaction. This observation indicates negligible, if any, formation of **a** during the course of the reaction. On the other hand, our research group and other groups have shown that a large excess of **a** (ca. 0.2–1 M) is required to drive the reductive amination of ketone substrates (15–50 mM) in aqueous buffer to a significant extent.[6–8, 10d, i] Moreover, AmDHs, such as Ch1-AmDH, have a K_M value of about 1 M for **a**.[10b] Similarly, with the only exception of glutamine dehydrogenases from bovine liver, frog liver and *Clostridium* SB₄, the parent wild-type amino acid dehydrogenases are also characterised by elevated K_M values for **a** (20–500 mM).[20] Consequently, biocatalytic reductive amination with **a** is kinetically disfavoured even at a significant concentration of **a** as an amine donor. Nonetheless, we investigated this possibility by incubating Rs-AmDH (102.8 μM) with **d** (50 mM) and NAD⁺ (60 mM) in phosphate buffer at pH 8.5, at 30 °C (Section 6.1 in the Supporting Information). The possible formation of **a** was determined indirectly by analytical quantification of the consumption of **d**. As expected, the concentration of **d** remained constant over 48 h; hence excluding any detectable formation of **a** through oxidative deamination of **d** catalysed by Rs-AmDH.

The second option predicts the elimination of an alcohol (Scheme 2 B; cyclopropanol in the example) during the possible catalytic cycle of the enzymatic reductive amination between the ketone (**1** in the example) and amine donor (**d**, in the example). Through careful monitoring of the reactions, the formation of cyclopropanol as a by-product was never observed. Analysis was accomplished by comparing the GC-MS chromatogram (i.e., retention times and fragmentation patterns) of authentic cyclopropanol as a reference compound with GC-MS chromatograms for the enzymatic reductive amination (for details, see Section 6.2 in the Supporting Information). Crucially, control experiments also revealed that cyclopropanol (used as reference compound) was stable in the reaction buffer (1 M, pH 8.5) at 30 °C and within the 48 h reaction time (Section 6.2 in the Supporting Information).

The last option predicts a promiscuous formal transamination through $NAD^+/NADH$ redox-mediated iminium isomerisation (Scheme 2 C). Firstly, we ascertained that the presence of the NAD coenzyme was critical for a possible formal transamination. Therefore, Rs-AmDH (102.6 μM) and ketone **1** (10 mM) were incubated in aqueous buffer of amine **d** (1 M, pH 8.5), but in the absence of NADH. As expected, we did not observe any formation of products (for details, see Section 6.3 in the Supporting Information). Then, to exclude any possible classical transamination reaction enabled by PLP as a cofactor, we also repeated the same experiment, but in the presence of exogenous PLP (0.5 mM). Even in this case, no formation of any product was observed. Finally, we undertook further experiments to prove the promiscuous enzymatic activity depicted in Scheme 2 C. In the first set of experiments, we incubated chemically synthesised racemic *N*-[1-(4′-fluorophenyl)propan-2-yl]cyclopropanamine (**1 d**) in aqueous buffer in the presence of NAD^+ (varying concentration from 2 to 20 mM) and Rs-AmDH. In this way, we aimed to create a dynamic equilibrium between all possible oxidative deamination pathways and reductive amination pathways (for schematic details, see Section 6.4 in the Supporting Information). Crucially, control experiments (i.e., without AmDH) showed that **1 d** was stable under these reaction conditions and no reaction was observed. In contrast, the incubation of **1 d** and NAD^+ with the AmDH produced measurable amounts of primary amine **1 a** (for details, see Table S6). The concentration of **1 a** detected was typically low (ca. 1 % conversion) because **1 a** was also in equilibrium with **1** (ca. 7 % conversion); the latter species is favoured because of the aqueous environment (schematic details are given in Section 6.4 in the Supporting Information). Thus, with the results from these experiments, we proved that Rs-AmDH converted the secondary amine *rac*-**1 d** into the primary amine (*R*)-**1 a**, which was the second part of the mechanism depicted in Scheme 2 C. Further kinetic resolution experiments (Section 6.4 in the Supporting Information) on *rac*-**1 d** catalysed by Rs-AmDH and with NAD oxidase (NOx) for NAD^+ recycling was also performed. Detailed analysis of the composition of the reaction mixture revealed that the enzyme was indeed capable of distinguishing between the two enantiomeric forms of **1 d**. In fact, the *ee* of remaining substrate **1 d** increased over time. After 48 h reaction time, remaining **1 d** was about 70 %, where-

as its *ee* was about 16 % (Table S7). If perfect kinetic resolution had occurred, the remaining *ee* should have been ca. 43 %. Thus, these data clearly demonstrate that, albeit one enantiomer of the secondary amine **1 d** is preferred, both enantiomers can be accepted by Rs-AmDH.

In conclusion, considering all of the results, the side-product formation of enantiopure primary amines originates through non-classical promiscuous transamination activity that is mediated by the NAD coenzyme. The expected ketone by-products, such as cyclopropanone, formaldehyde or acetaldehyde could not be observed because of their known elevated instability and reactivity in solution.

## Elucidation of the stereoselective properties of AmDHs with the aid of computational studies

The models of Rs-AmDH previously discussed served as starting points for a deeper understanding of how a given substrate interacts with the active-site residues of the enzyme, while adapting its putative reactive pose(s). This information was used in the subsequent molecular modelling of Ch1-AmDH described in this paragraph. In fact, for in-depth computational analysis with the aim of elucidating the experimental observations regarding the stereoselectivity of the AmDHs, we selected the reaction between a ketone (**1**) and **b**, which was catalysed by Ch1-AmDH. This choice was made because data for conversion and *ee* of the reaction between **1** and **b** were available (Table 1, entries 1 and 2). Therefore, direct comparison between computational data and experimental laboratory data was possible.

Because the crystal structure of Ch1-AmDH is not publicly available, the initial step was to generate a high-quality homology model of this enzyme. The model of Ch1-AmDH was generated in two steps. Firstly, an "exploratory homology modelling run" was executed to determine what was (were) the most suitable template(s) for this enzyme. Secondly, a "productive homology modelling run" was executed by only considering the "best" template(s) as candidate(s) (for details, see the Experimental Section and Section 5.2 in the Supporting Information). It is noteworthy that our homology model was created with the enzyme in its reactive conformation (i.e., "closed conformation"), in which the NAD coenzyme is bound in the active site. This is an important prerequisite for performing molecular docking simulation with these enzymes, as described herein. In contrast, the available crystal structure of ODHs, which also catalyse the formation of secondary amine functionalities following a formally similar mechanism, are reported in the non-reactive conformation ("open conformation"), in which the NAD coenzyme is unfortunately absent.[16c]

We initially performed molecular docking simulations by using the obtained model of Ch1-AmDH as a target with iminium intermediates **1 a*** and **1 b*** as ligands (that is, **1 a*** and **1 b*** are generated by the interaction between the ketone **1** with **a** or **b**, respectively). The aim was to obtain models of possible reactive conformations that explained the differences in stereoselectivity of the reaction, considering the formation of the *R*-configured enantiopure primary amine through the

reaction of **1** with **a**[10b,d] or both secondary amine enantiomers through the reaction of **1** with **b**. Through analysis of the structures obtained from molecular docking simulations, we were able to create the putative pro-*R* and pro-*S* binding modes for both iminium intermediates: **1a*** and **1b***. Comparing the models of Ch1-AmDH possessing **1a*** bound either in pro-*S* or in pro-*R* reactive conformations, the calculated binding energies and calculated distances between the departing hydride of NADH and the prochiral carbon of the iminium intermediate (distance 1, as defined in Figure 2) were similar. A similar scenario was also observed in models of Ch1-AmDH exhibiting **1b*** bound either in pro-*S* or in pro-*R* reactive conformations. Thus, we executed a set of molecular dynamics (MD) simulations with the aim of "relaxing" the docked enzyme–substrate complexes and, therefore, allowing for a more accurate re-evaluation of the reactive conformations for **1a*** and **1b*** (Figure 3 A and B and Section 5.2 in the Supporting Information). After MD relaxation, it was evident that Ch1-AmDH did not tolerate **1a*** in the pro-*S* binding mode well (Figure S6 A and B, Section 5.2 in the Supporting Information); hence, the pro-*R* binding mode was highly preferred for **1a***. After MD conformational relaxation, Figure 3 C and D has been created and depicts: 1) the average relative binding energies for the binding of the imine intermediates (pro-*S* **1a***, pro-*R* **1a***, pro-*S* **1b*** and pro-*R* **1b***) in the active site of Ch1-AmDH; and 2) the average distances between the departing hydride of NADH and the pro-chiral carbon of the imine intermediates (distance 1, as previously defined). The pro-*S* binding conformation of **1a*** is less favoured, relative to all other binding conformations (Figure 3 C) that appear to be energetically similar. More instructive is an analysis of the behaviour of distance 1 over the time of the simulations. Substrate intermediate **1a*** in the pro-*R* conformation showed an average distance 1 of (2.90 ± 0.20) Å, whereas in the pro-*S* conformation this distance had moved considerably above the threshold distance, with an average of (3.74 ± 0.64) Å. Slightly similar behaviour was ob-
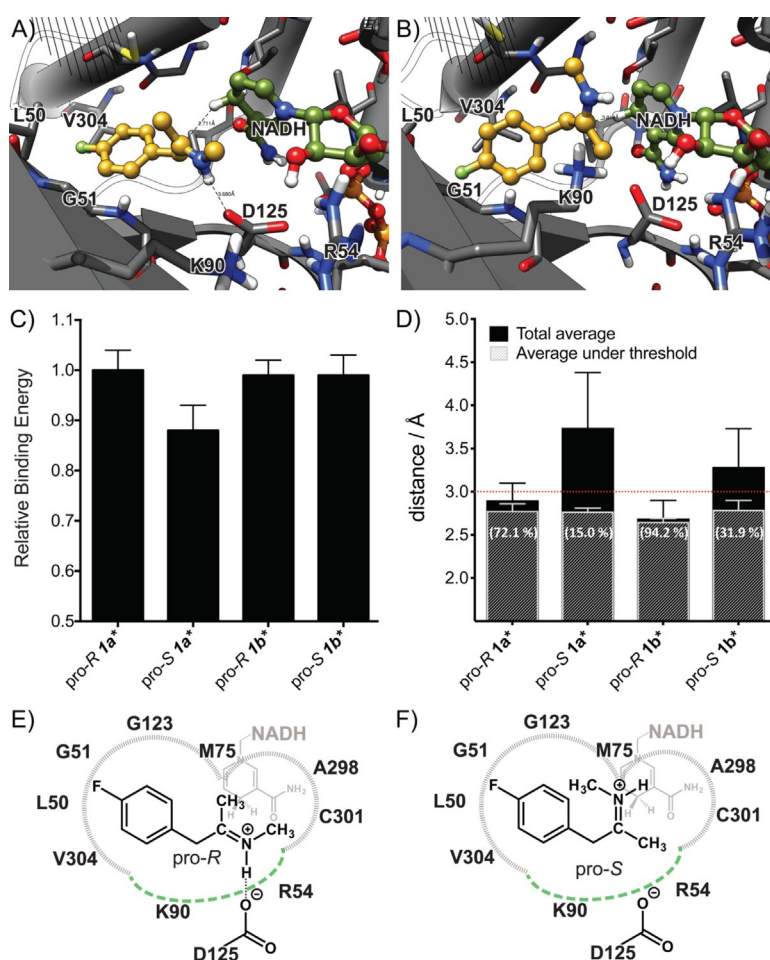

Figure 3. Pro-chiral preferences of Ch1-AmDH. Representative relaxed MD snapshots of **1b*** in A) pro-*R* and B) pro-*S* conformations. The substrate is shown in yellow, whereas NADH is shown in green. For clarity, no nonpolar hydrogen atoms were shown. C) Relative binding energy for **1a*** and **1b*** on their pro-*R* and pro-*S* configurations. All binding energies are given relative to the average binding energy of **1a*** in the pro-*R* conformation. A lower value of relative binding energy means less favourable binding. Only those snapshots that showed the substrate in its reactive conformation were considered for binding energy determination. D) Distance from the departing hydride of the coenzyme (NADH) to the pro-chiral carbon of the ligand (iminium) for **1a*** and **1b*** (in both pro-*R* and pro-*S* configurations). The numbers in parentheses indicate the percentage of snapshots that contributed with substrates located under the distance threshold (3 Å). Observed enzyme/substrate contacts for **1b*** in E) pro-*R* and F) pro-*S* conformations. Lines in grey indicate hydrophobic interactions, whereas the dashed green lines indicate hydrophilic interactions. The NADH cofactor is depicted behind the substrate in light grey.

served for the substrate intermediate **1b***, which showed an average distance 1 value of (2.69±0.11) Å in the pro-*R* conformation, but a higher average distance value of (3.29±0.36) Å in the pro-*S* conformation. Nevertheless, it is important to note that distance 1 for pro-*S* **1b*** ((3.29±0.36) Å) is shorter than that of the same distance for pro-*S* **1a*** ((3.74±0.64) Å). This finding indicates that Ch1-AmDH must tolerate the pro-*S* conformation of **1b*** better than the pro-*S* conformation of **1a***. On the other hand, intermediate **1b*** in the pro-*R* orientation is still the preferred binding mode by Ch1-AmDH. This can be observed further in Figure 3D, in which approximately 94% of the MD snapshots (within the simulation time) represent the pro-*R* **1b*** intermediate in the active site of Ch1-AmDH with a distance between the prochiral carbon atom and attacking hydride of NADH (distance 1, as previously defined) below the threshold of 3 Å (required for a hydride shift). Thus, there is an elevated probability that the hydride shift from NADH to **1b*** occurs if **1b*** is bound in the pro-*R* binding conformation. Conversely, the pro-*S* binding conformation of **1b*** is less favourable for a hydride shift from NADH because only approximately 32% of the MD snapshots showed a distance 1 value below the threshold of 3 Å.

On the other hand, the relative binding energies of **1b*** in pro-*R* and pro-*S* conformations, respectively, seem to be approximately the same (Figure 3C). We can therefore conclude that, although tolerated, the pro-*S* configuration of **1b*** has a lower probability of reacting than that of the pro-*R* counterpart. The pro-*S* conformation of **1b*** seems to be stabilised by hydrophobic interactions of the methyl group with residues M75, A298 and C310. The pro-*R* binding mode of **1b*** is stabilised as already reported in the literature for wild-type aromatic amine dehydrogenases.[17] This stabilisation involves the previously discussed highly conserved Asp residue (numbering 125 for Ch1-AmDH) in a similar way as that depicted in Figure 2 for Rs-AmDH. The described enzyme/substrate contacts for Ch1-AmDH are depicted in Figure 3E and F for both pro-*R* and pro-*S* binding modes. It is interesting to note that intermediate **1b*** bound in its reactive pro-*R* binding mode was mainly observed by assuming the *E* configuration at the C=N double bond (Figure 3A and E). In contrast, intermediate **1b*** bound in its reactive pro-*S* binding mode was mainly observed by assuming the *Z* configuration (Figure 3B and F). It is known from reports in the literature that *N*-alkylimines can isomerise in solution at ambient temperature through tautomerisation and rotation.[21] In the case of intermediate **1b***, which bears non-bulky substituents, such as hydrogen or methyl groups, the *E* isomer is known to be favoured in equilibrium in solution at room temperature.[22] Nonetheless, in our case, the enzyme selects the preferred *E* or *Z* configuration of the intermediate in the active site.

Additionally, a non-bonding dihedral angle (χ) was defined to describe the stereo-binding mode of the substrate in the active site (Figure 4A). This dihedral angle was defined by following the Cahn–Ingold–Prelog (C.I.P.) priority rules between the three atoms bonded to the pro-chiral carbon of the substrate and the hydride atom of the NADH cofactor. This dihedral angle was determined for the *R*- and *S*-configured prod-
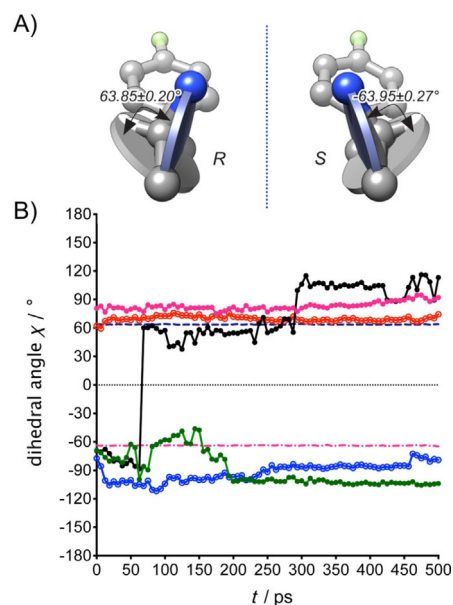
Figure 4. Dihedral angle, χ, versus time for the MD simulations starting from pro-*R* **1a***, pro-*S* **1a***, pro-*R* **1b*** and pro-*S* **1b***. A) Illustrative depiction of χ for the *R*- and *S*-configured product of the reaction. These values were used as a reference to describe the hydride shift from NADH that would afford any of these enantiomers. According to this definition, a positive value of the dihedral angle in the intermediate will lead to the *R*-configured amine upon reduction. A negative value will lead to the *S*-configured amine upon reduction. B) The average variation of χ over the time is shown for simulations of pro-*R* **1a*** (●), pro-*S* **1a*** (no shift: ● or *S*→*R* shift: ●), pro-*R* **1b*** (○) and pro-*S* **1b*** (○). For each system, the depicted line is the average of six independent simulation runs (all simulation runs are reported in Figure S7). Only simulation run number 5 for substrate **1a*** in the pro-*S* binding conformation was not considered for the average calculation because the substrate moved away from the active site (Figure S7B). For the sake of clarity of the depiction, the error bars of these average simulations have been omitted (Figure S7). The average χ values for the *R*- (-----) and *S*-configured products (-·-·-) are also shown as dashed lines.

ucts (both for **1a** and **1b**) of the reaction; thus indicating that the *R*-configured product shows an average value of (63.85±0.20)°, whereas the *S*-configured product shows an average value of (−63.95±0.27)°.

Figure 4B shows the behaviour of χ as a function of time for substrate intermediates **1a*** and **1b*** and starting from both pro-*R* and pro-*S* binding conformations. Notably, for the intermediate substrate **1a*** bound in a pro-*S* binding mode, a switch to the pro-*R* conformation occurred within the simulation time (Figure 4B; for details see Section 5.2 and Figure S7B in the Supporting Information; see also in the Supporting Information movie file "switch_pro-S_to_pro-R_primary_imine.avi"). In particular, 50% of the simulation runs for pro-*S* **1a*** (3 out of 6) showed this switch from pro-*S* to pro-*R* (Figure 4B, black line). An additional simulation (run 5) also showed a switch in the conformation, but, during this simulation, the substrate moved out of the active site. Therefore, we did not consider this simulation in the calculation of the average values. Only in two cases out of six did substrate **1a*** maintain the pro-*S* binding conformation (Figure 4B, green line). In contrast to the simulation with pro-*S* **1a***, a conformational switch was never observed for simulations starting from either pro-*R*

1a* (pink line) or pro-R 1b* (orange line) or pro-S 1b* (blue line, Figure 4B; for details see Section 5.2 and Figure S7A, C and D). It is important to note that the average value of the herein defined dihedral angle for pro-S 1a* amongst simulation runs has only an illustrative value; thus indicating great conformational changes in the active site of Ch1-AmDH.

In summary, the MD simulations provide an insight at the molecular level on different stereoselective behaviour of the AmDHs in the reductive amination of prochiral ketones with either a or more complex amines. If a is the amine donor, the reactive pro-R conformation of the iminium intermediate is much more favoured than that of the pro-S conformation, which explains why the primary amine product is always experimentally obtained in enantiopure R-configured form.[10d] In the event that a pro-S binding mode for the primary iminium intermediate is generated in the active site, a conformational switch to pro-R binding mode (Figure 4B, black line; see also the Supporting Information movie file "switch_pro-S_to_pro-R_primary_imine.avi") or even the release of the intermediate from the active site is likely to occur. Conversely, if a primary amine is the amine donor for reductive amination, both pro-R and pro-S binding modes can be generated as reactive conformations, so that the secondary amine product is obtained in both enantiomeric forms.
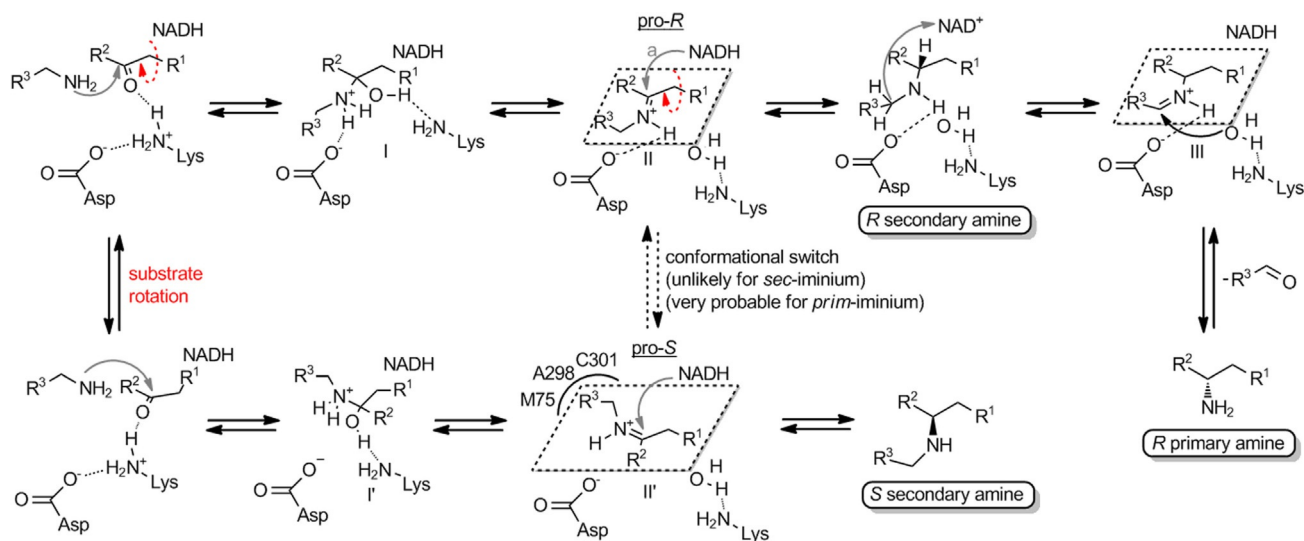
Proposed catalytic mechanism

Considering all results obtained from practical experimental laboratory and computational experiments, we postulated a biocatalytic cycle that illustrates the formation of both secondary and primary amines (Scheme 3). The proposed cycle is adapted from the catalytic mechanism of phenylalanine dehydrogenases from *Rhodococcus* sp. M4 (the wild-type parent of the variant Rs-AmDH).[17]

In the first step, the carbonyl compound and amine donor generate the geminal amino alcohol (I or I') assisted by protonated Lys and deprotonated Asp residues from the AmDH active site. Intermediates I and I' can interconvert through rotation around the carbon–carbon bond that connects the prochiral sp2-carbon of the ketone and the sp3-carbon in the α position (the latter is connected to substituent R1 in Scheme 3). This rotation appears to be the most probable one because our model structures clearly show that the R1 substituent (e.g., in this study phenyl, phenylmethyl, alkyl) is tightly accommodated in a hydrophobic cavity in the active site of the AmDH (Figure 5).

Then, assisted by the same Lys residues, a water molecule is released from intermediates I or I' to generate iminium intermediates II (pro-R binding mode) and II' (pro-S binding mode), respectively. From the analysis of the snapshots of our molecular docking simulations, it appears that the iminium moiety of intermediate II (pro-R) is stabilised further by a hydrogen bond with the deprotonated aspartate residue (Figure 3A and E; Asp118 in Rs-AmDH or Asp125 in Ch1-AmDH). In contrast, such a hydrogen bond was not observed with intermediate II' because the aspartate residue was too distant from the hydrogen of the iminium moiety. Intermediate II' appears to be stabilised by hydrophobic interactions of the methyl group with residues M75, A298 and C310 (Figure 3B and F). As observed previously, intermediate II assumes the preferred E configuration, whereas intermediate II' assumes the preferred Z configuration (Scheme 3, C.I.P. priority: R1 > R2). Although a conforma-

Scheme 3. Proposed catalytic cycle for reductive amination catalysed by Rs-AmDH and Ch1-AmDH with amine donors different from a (adapted from ref. [17]. Copyright: 2000, American Chemical Society). Two stereocomplementary binding modes are the most probable: either intermediate II (E configuration and pro-R binding mode) or intermediate II' (Z configuration and pro-S binding mode). Interconversion between II and II' (and vice versa) was never observed for secondary iminium intermediates during the time of our simulations. In contrast, interconversion from II' to II was observed in 50% of cases in our simulations with primary iminium intermediates. The opposite interconversion (from II to II') was never observed. Further reduction of intermediate II' through a hydride shift from NADH forms the secondary amine product in the S configuration. Reduction of intermediate II by a hydride shift from NADH forms the secondary amine product in the R configuration. However, intermediate II can also be re-oxidised to iminium isomer III. After this formal imine isomerisation step, the hydrolysis of intermediate III yields the primary amine product in the R configuration.
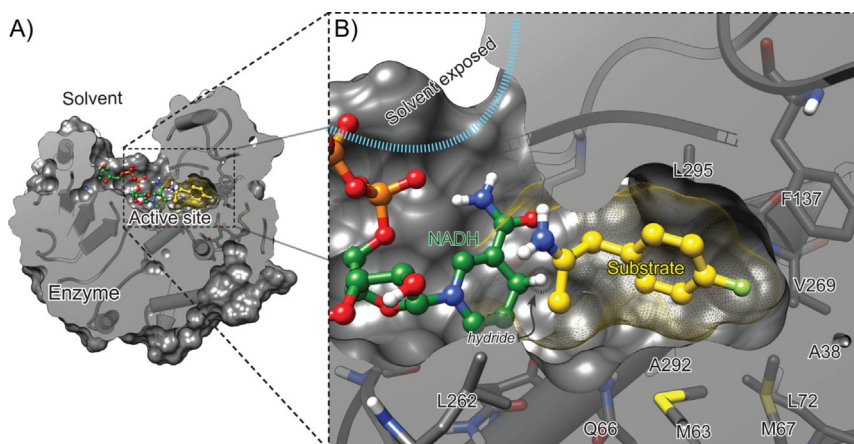
Figure 5. A) Hydrophobic binding pocket of RsAmDH. B) Amino acid residues constituting the hydrophobic binding pocket in the active site of Rs AmDH.

tional switch from pro-*S* to pro-*R* binding mode (or vice versa) of the secondary imine intermediate was never observed within the time of our simulations, this event cannot be completely ruled out. Hence, this theoretically possible conformational binding switch is depicted as a dashed arrows in Scheme 3. In contrast, as previously described, such a conformational binding switch from pro-*S* to pro-*R* (but not vice versa) is very likely to occur with primary iminium intermediates (Figure 4B; see also the Supporting Information movies).

At this stage, a hydride shift from NADH to intermediates **II** or **II′** can occur to give the secondary amine product in *R* or *S* configurations, respectively. Nonetheless, amine (*R*)-**1b**, obtained by the reduction of intermediate **II**, can also be subjected to further promiscuous re-oxidation in the active site by abstraction of the hydride from the other alkyl chain of the amine moiety. This promiscuous formal imine isomerisation generates intermediate **III**. Hydrolysis of intermediate **III** by the same water molecule coordinated to the catalytic Lys residue or by another polarised water molecule at an appropriate distance in the active site forms the primary amine product (*R*)-**1b** as a single enantiomer.

Conclusion

Known AmDHs were engineered from amino acid dehydrogenases, and therefore, they displayed the highest catalytic activity with **a** as an amine donor. In contrast to the common belief that **a** is the only possible amine donor, we have demonstrated herein that the reactivity of AmDHs can be extended to other amine donors. In fact, enantioenriched secondary amines were obtained with conversions of up to 43%. However, we observed that control of the chemo- and stereoselectivity of the reductive amination catalysed by AmDHs with different amine donors was challenging. This study revealed that the secondary amine products could only be obtained in enantioenriched form, so far. Furthermore, an unprecedented NAD-dependent isomerisation step may take place in the active site of the enzyme, during the catalytic cycle, ultimately leading to the formation of the structurally related enantiopure primary amine as an additional product. To the best of our knowledge,

our findings suggest the first example of a formal enzymatic transamination mechanism that is not catalysed by PLP. By combining practical laboratory experiments and computational experiments and analysis, we could rationalise the formation of all products observed in the reaction mixture. Finally, a catalytic cycle was postulated based on the known natural catalytic cycle of the wild-type phenylalanine dehydrogenases from *Rhodococcus* sp. M4.

In summary, this study provides an understanding of the molecular discriminants that are crucial for the efficient catalytic activity of AmDHs, and it will contribute to providing knowledge required for further rational engineering of AmDHs to improve activity, stereoselectivity and suppress possible side reactions.

Experimental Section

For general information, materials, details on computational molecular modelling, chemical synthesis of references compounds and analytics, see the Supporting Information.

General procedure for the biocatalytic amination of carbonyl compounds 1–13 with amine donors b–j: All buffers were prepared by dissolving amine donors **b–k** (Figure S2) in distilled water to obtain a final concentration of 1 M. The pH was adjusted to 8.5 with formic acid. In the case of aniline (**l**), due to solubility issues, a saturated solution (pH 8.5) was used. Both Rs-AmDH and Ch1-AmDH were tested for the synthesis of secondary or tertiary amines by using all 11 different amine buffers, as well as carbonyl compounds **1–12** as acceptor substrates (for detailed structures, see Figure S1).

Biotransformations were performed in 1.5 mL Eppendorf tubes with a total reaction volume of 0.5 mL. The reaction consisted of NAD$^+$ (1 mM), substrate (10 mM), AmDH (102.8 μM for Rs-AmDH and 91.8 μM for Ch1-AmDH) and Cb-FDH (23.5 μM). Reactions were performed at 30 °C for 48 h on orbital shakers (170 rpm) in a horizontal position. The reactions were quenched after 48 h by the addition of an aqueous solution of KOH (10 M, 100 μL). Then, the organic compounds were extracted with dichloromethane (CH$_2$Cl$_2$, 1×600 μL) and dried with magnesium sulfate. The conversions were measured by means of GC-FID by using commercially available or chemically synthesised reference compounds. If reference

compounds were not available, preliminary identification of the desired products (amines) was also achieved by means of GC-MS by using the same column and method as that for GC-FID. The *ee* value was determined after derivatisation to an acetamido by using a solution of 4-dimethylaminopyridine (DMAP; 50 mg) in acetic anhydride (1 mL, 409 mM). In total, 50 μL of this solution was added to each solution of the amine product in 600 μL dichloromethane. The mixtures were shaken at 25 °C for 30 min. After that, water (500 μL) was added for another 30 min with shaking at 25 °C. The samples were centrifuged for 10 min at 14 800 rpm, and the organic phases were dried with magnesium sulfate prior to injection in the Chrompack Chiracel Dex-CB (25 m, 320 μm, 0.25 μm, Agilent) or Hydrodex-β-TBDAC systems (50 m, 0.40 mm, 0.25 mm, Macherey–Nagel).

Computational molecular modelling

Computational model of Rs-AmDH: The 3D structural model of Rs-AmDH was created starting from the crystal structure of L-phenylalanine dehydrogenase from *Rhodococcus* sp. M4 (PDB ID: 1C1D).[17] The Rs-AmDH variant differed only for three amino acid positions, namely, K66Q, S149G and N262C, from the wild-type L-phenylalanine dehydrogenase.[7] These mutations were induced in silico by using YASARA software[23] with the AMBER 03 force field.[24] The protonation state of all atoms was automatically adjusted, with the exception of those atoms involved in hydride transfer between the co-factor and substrate. The protonation state of the latter atoms was adjusted manually accordingly. Every time a mutation was induced, a three-step energy minimisation was executed. Step one: only the mutated residue was energetically minimised. Step two: the mutated residue plus all those residues within a radius of 6 Å of the mutated residue were subjected to energy minimisation. Step three: the complete enzyme was submitted to energy minimisation. By using this energy minimisation protocol, a gradual adjustment of the complete structure to the new mutation was assured; thus avoiding the production of undesired deformations of the secondary structure.

All selected substrates were generated in situ by mimicking the observed position of L-phenylalanine in the crystal structure (PDB ID: 1C1D). After substrate generation, the three-step energy minimisation protocol described above was applied. These models were created to study possible reactive poses of Rs-AmDH containing the ketimine (Figure S4) and aldimine (Figure S5) intermediates formed during the catalytic mechanism. Based on the reported catalytic mechanism of the parent wild-type L-phenylalanine dehydrogenase from Rhodococcus sp. M4,[17] we analysed the models by considering two crucial parameters: 1) the distance between the attacking hydride of NADH and the pro-chiral carbon of the iminium intermediate (distance 1); and 2) the distance between the negatively charged oxygen atom of the terminal carboxylic group of D118 in Rs-AmDH and the hydrogen of the iminium group (distance 2). For details and figures, see Section 5.1 in the Supporting Information.

Computational model of Ch1-AmDH: The Ch1-AmDH chimeric enzyme was previously created in the laboratory through domain shuffling of two first-generation variants, such as Bb-PhAmDH (originating from *B. badius* L-phenylalanine dehydrogenase) and L-AmDH (originating from *Bacillus stearothermophilus* L-leucine dehydrogenase).[10b] The Ch1-AmDH model structure was generated in two steps. Firstly, an exploratory homology modelling run was executed to determine the most suitable template(s) for this enzyme. Then, a second homology modelling run was executed by only considering the best template(s) as candidate(s).

Exploratory homology modelling run: This exploratory run was performed by using the YASARA[23] homology model building protocol,[25] which involved multi-template structural model generation. Because the linear amino acid sequence of the target protein was the only given input, possible templates were identified by running three PSI-BLAST[26] iterations to extract a position-specific scoring matrix (PSSM) from UniRef90,[27] and then searching the PDB for a match with an *E* value below the homology modelling cut-off of 0.005. A maximum of five templates were allowed. To aid alignment correction and loop modelling, secondary structure prediction for the target sequence had to be obtained. This was achieved by running PSI-BLAST to create a target sequence profile and feeding it to the PSI-Pred[28] secondary structure prediction algorithm. For each of the templates found, models were built. Either a single model per template was generated, if the alignment was certain, or a number of alternative models were generated, if the alignment was ambiguous. A maximum of 50 conformations per loop were explored. A maximum of 10 residues were added to the termini. Finally, YASARA attempted to combine the best parts of the generated models to obtain a hybrid model, with the intention of increasing the accuracy beyond each of the contributors. The quality of the models was evaluated by the use of the *Z* score.[29] A *Z* score describes how many standard deviations the model quality is away from the average high-resolution X-ray structure. The overall *Z* scores for all models were calculated as the weighted averages of individual *Z* scores by using the formula Overall = $0.145 \times$ Dihedrals + $0.390 \times$ Packing1D + $0.465 \times$ Packing3D. The overall score thus captures the correctness of backbone (Ramachandran plot) and side-chain dihedral angles, as well as packing interactions.

Production homology modelling run. Based on the results of the exploratory run, it turned out that the generated model was of reasonably good quality; however, it contained neither the co-factor nor a co-crystallised substrate in its active site. For this reason, the template crystal structure (1C1D) was only considered for the production run. In fact, the crystal structure contained co-crystallised cofactor and substrate in the active site.[17] In summary, the production run was performed by using the same parameters as those used in the exploratory run, with the exception of the following parameters: only one template was manually selected, a maximum of 100 conformations per loop were explored and a maximum of two residues were added to the termini. To increase their quality, the obtained models were submitted to 500 ps MD refinement simulation by using the protocol described by Krieger et al.[30] A structural snapshot was saved every 25 ps for further analysis of quality parameters (potential energy, Dihedrals, Packing1D and Packing3D). The model with the best quality was selected for further computational molecular studies. The results of homology model generation are reported in Table S4.

Computational molecular docking and MD simulations: The model of Ch1-AmDH obtained in the previous step was used as the starting point for MD simulations. MD simulations were executed by using the YASARA software,[23] with the AMBER 03 force field.[24] Prior to this, all substrates were generated in situ starting from the reactive pose of L-phenylalanine. After substrate generation, the three-step energy minimisation protocol was applied. These models were created by representing the reactive pose of Ch1-AmDH with the iminium intermediate. The final relaxed structure was evaluated by using the Autodock Vina[31] scoring function to assess its binding energy at the reactive pose. Both binding conformations, pro-*R* and pro-*S*, obtained were submitted to MD simulations. A minimum of six independent MD simulations (with random initial velocities) were executed per system. Each MD simu-

lation was run for 500 ps, and a snapshot was taken every 6.25 ps; thus resulting in 81 frames (counting the starting structure) per simulation. These frames were submitted for analysis and several dynamic properties were followed. However, the distance between the departing hydride of NADH and the pro-chiral carbon atom of the imine intermediate substrate was considered as the main descriptor of the reactive pose. The sum of the vdW radii[18] of carbon and hydrogen was considered as the threshold distance, which was set to a rounded value of 3.0 Å ($r_H^{vdW} = 1.2$ Å, $r_C^{vdW} = 1.7$ Å; $r_H^{vdW} + r_C^{vdW} = 2.9$ Å; thus: $d_{CH}^{threshold} = 3.0$ Å).

Acknowledgements

Conflict of Interest

The authors declare no conflict of interest.

[1] a) O. Khersonsky, D. S. Tawfik, *Annu. Rev. Biochem.* **2010**, *79*, 471–505; b) I. Nobeli, A. D. Favia, J. M. Thornton, *Nat. Biotechnol.* **2009**, *27*, 157–167; c) M. S. Humble, P. Berglund, *Eur. J. Org. Chem.* **2011**, 3391–3401; d) K. Hult, P. Berglund, *Trends Biotechnol.* **2007**, *25*, 231–238; e) O. Khersonsky, C. Roodveldt, D. S. Tawfik, *Curr. Opin. Chem. Biol.* **2006**, *10*, 498–508; f) U. T. Bornscheuer, R. J. Kazlauskas, *Angew. Chem. Int. Ed.* **2004**, *43*, 6032–6040; *Angew. Chem.* **2004**, *116*, 6156–6165; g) A. Babtie, N. Tokuriki, F. Hollfelder, *Curr. Opin. Chem. Biol.* **2010**, *14*, 200–207; h) R. J. Kazlauskas, *Curr. Opin. Chem. Biol.* **2005**, *9*, 195–201.

[2] a) J. Vilím, T. Knaus, F. Mutti, *Angew. Chem. Int. Ed.* **2018**, *57*, 14240–14244; b) M. A. Emmanuel, N. R. Greenberg, D. G. Oblinsky, T. K. Hyster, *Nature* **2016**, *540*, 414–417; c) B. A. Sandoval, A. J. Meichan, T. K. Hyster, *J. Am. Chem. Soc.* **2017**, *139*, 11313–11316; d) X. Garrabou, T. Beck, D. Hilvert, *Angew. Chem. Int. Ed.* **2015**, *54*, 5609–5612; *Angew. Chem.* **2015**, *127*, 5701–5704; e) A. Cuetos, M. Garcia-Ramos, E. M. Fischereder, A. Diaz-Rodriguez, G. Grogan, V. Gotor, W. Kroutil, I. Lavandera, *Angew. Chem. Int. Ed.* **2016**, *55*, 3144–3147; *Angew. Chem.* **2016**, *128*, 3196–3199; f) D. Wetzl, J. Bolsinger, B. M. Nestl, B. Hauer, *ChemCatChem* **2016**, *8*, 1361–1366; g) Z. Liu, Y. Lv, A. Zhu, Z. An, *ACS Macro Lett.* **2018**, *7*, 1–6; h) S. E. Payer, X. Sheng, H. Pollak, C. Wuensch, G. Steinkellner, F. Himo, S. M. Glueck, K. Faber, *Adv. Synth. Catal.* **2017**, *359*, 2066–2075; i) P. S. Coelho, E. M. Brustad, A. Kannan, F. H. Arnold, *Science* **2013**, *339*, 307–310; j) G. D. Roiban, M. T. Reetz, *Angew. Chem. Int. Ed.* **2013**, *52*, 5439–5440; *Angew. Chem.* **2013**, *125*, 5549–5550; k) Y. Miao, E. M. Geertsema, P. G. Tepper, E. Zandvoort, G. J. Poelarends, *ChemBioChem* **2013**, *14*, 191–194; l) C. Wuensch, J. Gross, G. Steinkellner, K. Gruber, S. M. Glueck, K. Faber, *Angew. Chem. Int. Ed.* **2013**, *52*, 2293–2297; *Angew. Chem.* **2013**, *125*, 2349–2353; m) T. Devamani, A. M. Rauwerdink, M. Lunzer, B. J. Jones, J. L. Mooney, M. A. Tan, Z. J. Zhang, J. H. Xu, A. M. Dean, R. J. Kazlauskas, *J. Am. Chem. Soc.* **2016**, *138*, 1046–1056; n) Y. Miao, R. Metzner, Y. Asano, *ChemBioChem* **2017**, *18*, 451–454; o) S. Roth, A. Prag, C. Wechsler, M. Marolt, S. Ferlaino, S. Ludeke, N. Sandon,

D. Wetzl, H. Iding, B. Wirz, M. Muller, *ChemBioChem* **2017**, *18*, 1703–1706.

[3] M. J. Abrahamson, E. Vazquez-Figueroa, N. B. Woodall, J. C. Moore, A. S. Bommarius, *Angew. Chem. Int. Ed.* **2012**, *51*, 3969–3972; *Angew. Chem.* **2012**, *124*, 4036–4040.

[4] F.-F. Chen, Y.-Y. Liu, G.-W. Zheng, J.-H. Xu, *ChemCatChem* **2015**, *7*, 3838–3841.

[5] F.-F. Chen, G.-W. Zheng, L. Liu, H. Li, Q. Chen, F.-L. Li, C.-X. Li, J.-H. Xu, *ACS Catal.* **2018**, *8*, 2622–2628.

[6] M. J. Abrahamson, J. W. Wong, A. S. Bommarius, *Adv. Synth. Catal.* **2013**, *355*, 1780–1786.

[7] L. J. Ye, H. H. Toh, Y. Yang, J. P. Adams, R. Snajdrova, Z. Li, *ACS Catal.* **2015**, *5*, 1119–1122.

[8] A. Pushpanath, E. Siirola, A. Bornadel, D. Woodlock, U. Schell, *ACS Catal.* **2017**, *7*, 3204–3209.

[9] O. Mayol, S. David, E. Darii, A. Debard, A. Mariage, V. Pellouin, J.-L. Petit, M. Salanoubat, V. de Berardinis, A. Zaparucha, C. Vergne-Vaxelaire, *Catal. Sci. Technol.* **2016**, *6*, 7421–7428.

[10] a) S. K. Au, B. R. Bommarius, A. S. Bommarius, *ACS Catal.* **2014**, *4*, 4021–4026; b) B. R. Bommarius, M. Schürmann, A. S. Bommarius, *Chem. Commun.* **2014**, *50*, 14953–14955; c) F. G. Mutti, T. Knaus, N. S. Scrutton, M. Breuer, N. J. Turner, *Science* **2015**, *349*, 1525–1529; d) T. Knaus, W. Böhmer, F. G. Mutti, *Green Chem.* **2017**, *19*, 453–463; e) J. Liu, B. Q. W. Pang, J. P. Adams, R. Snajdrova, Z. Li, *ChemCatChem* **2017**, *9*, 425–431; f) T. Knaus, L. Cariati, M. F. Masman, F. G. Mutti, *Org. Biomol. Chem.* **2017**, *15*, 8313–8325; g) H. Ren, Y. Zhang, J. Su, P. Lin, B. Wang, B. Fang, S. Wang, *J. Biotechnol.* **2017**, *241*, 33–41; h) M. P. Thompson, N. J. Turner, *ChemCatChem* **2017**, *9*, 3833–3836; i) W. Böhmer, T. Knaus, F. G. Mutti, *ChemCatChem* **2018**, *10*, 731–735; j) J. Löwe, A. A. Ingram, H. Gröger, *Bioorg. Med. Chem.* **2017**, *26*, 1387–1392.

[11] a) J. H. Schrittwieser, S. Velikogne, W. Kroutil, *Adv. Synth. Catal.* **2015**, *357*, 1655–1685; b) M. Sharma, J. Mangas-Sanchez, N. J. Turner, G. Grogan, *Adv. Synth. Catal.* **2017**, *359*, 2011–2025.

[12] a) P. N. Scheller, M. Lenz, S. C. Hammer, B. Hauer, B. M. Nestl, *ChemCatChem* **2015**, *7*, 3239–3242; b) T. Huber, L. Schneider, A. Präg, S. Gerhardt, O. Einsle, M. Müller, *ChemCatChem* **2014**, *6*, 2248–2252; c) D. Wetzl, M. Gand, A. Ross, H. Müller, P. Matzel, S. P. Hanlon, M. Müller, B. Wirz, M. Höhne, H. Iding, *ChemCatChem* **2016**, *8*, 2023–2026; d) P. Matzel, M. Gand, M. Höhne, *Green Chem.* **2017**, *19*, 385–389.

[13] a) G. A. Aleku, S. P. France, H. Man, J. Mangas-Sanchez, S. L. Montgomery, M. Sharma, F. Leipold, S. Hussain, G. Grogan, N. J. Turner, *Nat. Chem.* **2017**, *9*, 961–969; b) S. L. Montgomery, J. Mangas-Sanchez, M. P. Thompson, G. A. Aleku, B. Dominguez, N. J. Turner, *Angew. Chem. Int. Ed.* **2017**, *56*, 10491–10494; *Angew. Chem.* **2017**, *129*, 10627–10630.

[14] S. P. France, R. M. Howard, J. Steflik, N. J. Weise, J. Mangas-Sanchez, S. L. Montgomery, R. Crook, R. Kumar, N. J. Turner, *ChemCatChem* **2018**, *10*, 510–514.

[15] H. Chen, J. C. Moore, S. J. Collier, D. Smith, J. Nazor, G. Hughes, J. Janey, G. Huisman, S. Novick, N. Agard, O. Alvizo, G. Cope, W.-L. Yeo, J. Sukumaran, S. Ng (Codexis-INC), WO2013/170050, **2013**.

[16] a) Y. Asano, K. Yamaguchi, K. Kondo, *J. Bacteriol.* **1989**, *171*, 4466–4471; b) Y. Kato, H. Yamada, Y. Asano, *J. Mol. Catal. B* **1996**, *1*, 151–160; c) Y. A. K. L. Britton, D. W. Rice, *Nat. Struct. Biol.* **1998**, *5*, 593–601.

[17] N. M. W. Brunhuber, J. B. Thoden, J. S. Blanchard, J. L. Vanhooke, *Biochemistry* **2000**, *39*, 9174–9187.

[18] R. S. Rowland, R. Taylor, *J. Phys. Chem.* **1996**, *100*, 7384–7391.

[19] a) S. Mathew, H. Yun, *ACS Catal.* **2012**, *2*, 993–1001; b) E. F. Oliveira, N. M. Cerqueira, P. A. Fernandes, M. J. Ramos, *J. Am. Chem. Soc.* **2011**, *133*, 15496–15505; c) P. K. Mehta, T. I. Hale, P. Christen, *Eur. J. Biochem.* **1993**, *214*, 549–561; d) B.-Y. Hwang, B.-K. Cho, H. Yun, K. Koteshwar, B.-G. Kim, *J. Mol. Catal. B* **2005**, *37*, 47–55.

[20] K. S. Toshihisa Ohshima, *Adv. Biochem. Eng./Biotechnol.* **1990**, *42*, 187–209.

[21] a) W. B. Jennings, D. R. Boyd, *J. Am. Chem. Soc.* **1972**, *94*, 7187–7188; b) J. E. Johnson, N. M. Morales, A. M. Gorczyca, D. D. Dolliver, M. A. McAllister, *J. Org. Chem.* **2001**, *66*, 7979–7985.

[22] J. Bjørgo, D. R. Boyd, C. G. Watson, W. B. Jennings, *J. Chem. Soc. Perkin Trans. 2* **1974**, 757–762.

[23] E. Krieger, G. Koraimann, G. Vriend, *Proteins Struct. Funct. Bioinf.* **2002**, *47*, 393–402.

[24] C. Oostenbrink, A. Villa, A. E. Mark, W. F. van Gunsteren, *J. Comput. Chem.* **2004**, *25*, 1656–1676.

[25] a) E. Krieger, S. B. Nabuurs, G. Vriend, *Methods Biochem. Anal.* **2003**, *44*, 509–523; b) H. Venselaar, R. P. Joosten, B. Vroling, C. A. B. Baakman, M. L. Hekkelman, E. Krieger, G. Vriend, *Eur. Biophys. J.* **2010**, *39*, 551–563.

[26] S. F. Altschul, T. L. Madden, A. A. Schäffer, J. Zhang, Z. Zhang, W. Miller, D. J. Lipman, *Nucleic Acids Res.* **1997**, *25*, 3389–3402.

[27] B. E. Suzek, H. Huang, P. McGarvey, R. Mazumder, C. H. Wu, *Bioinformatics* **2007**, *23*, 1282–1288.

[28] D. T. Jones, *J. Mol. Biol.* **1999**, *292*, 195–202.

[29] a) R. A. Laskowski, M. W. MacArthur, D. S. Moss, J. M. Thornton, *J. Appl. Crystallogr.* **1993**, *26*, 283–291; b) R. W. Hooft, G. Vriend, C. Sander, E. E. Abola, *Nature* **1996**, *381*, 272–272.

[30] E. Krieger, T. Darden, S. B. Nabuurs, A. Finkelstein, G. Vriend, *Proteins Struct. Funct. Bioinf.* **2004**, *57*, 678–683.

[31] O. Trott, A. J. Olson, *J. Comput. Chem.* **2010**, *25*, 1656–1676.